PHYSICAL REVIEW B VOLUME 21, NUMBER 8 15 APRIL 1980

Electron diffraction from superlattices in graphite-rubidium intercalation compounds

N. Kambe,* G. Dresselhaus,† and M. S. Dresselhaus*
Massachusetts Institute of Technology, Cambridge, Massachusetts 02139
(Received 8 October 1979)

Electron-diffraction results are reported in the temperature range $110 < T < 900$ K for graphite-Rb intercalation compounds based on highly oriented pyrolytic graphite host material. Annealed stage $n = 1$ samples show the simple graphite pattern below ~ 300 K, corresponding to a $p(2 \times 2)R\,0°$ in-plane intercalate superlattice ordering with $\alpha,\beta,\gamma,\delta$ interlayer intercalate stacking order. A reversible transition is made at ~ 300 K to a $p(2 \times 2)R\,0°$ superlattice, but lacking $\alpha,\beta,\gamma,\delta$ stacking. The higher-stage compounds ($n = 2,3,4,7$) exhibit commensurate $p(\sqrt{7} \times \sqrt{7})R \pm 19.1°$ superlattices below a temperature T_U which decreases with increasing stage index from 170 K for $n = 2$. As T is increased above T_U, the higher-stage compounds exhibit a reversible transition to another ordered structure which is present until the transition to a high-temperature phase, observed at 620 K for $n = 2$. The structural transition at T_U between the two ordered phases is accompanied by a dramatic change in the bright-field real-image micrograph, taken on the same portion of the sample as the electron-diffraction patterns. The observation of a second ordered phase above T_U in the Rb compounds is in contrast with the disordered phase reported previously for second-stage K compounds.

I. INTRODUCTION

Of the various intercalation compounds that have been prepared, graphite intercalation compounds are of particular interest because of their high degree of intralayer and interlayer order. The occurrence of the staging phenomenon is the most striking aspect of this ordering and has received a great deal of attention. Graphite intercalation compounds, however, have other types of structural ordering, and these have received lesser attention. Among these, the in-plane ordering, in particular, is vital for the detailed interpretation of lattice mode structure[1,2] and electronic band structure,[3,4] topics that are now under active investigation. Study of in-plane ordering has led to the identification of a close relation between the structure of the intercalate and graphitic layers of the intercalation compounds with the corresponding layers in their parent materials.[5,6] This identification leads to important simplifications in the development of quantitative techniques for the interpretation of experimental data pertinent to the electronic structure and phonon dispersion relations for graphite intercalation compounds.

X-ray-diffraction,[7-10] electron-diffraction,[11-14] and neutron-diffraction[15] experiments provide the most sensitive methods for the determination of the structural ordering in graphite intercalation compounds. Because of practical considerations, the information provided by these techniques is in fact complementary. The only complete structural determinations that are currently available are for the stage-1 alkali-metal compounds C_8K, C_8Rb, C_8Cs,[7,8,16] and C_6Li,[17,18] and almost all these determinations have been made using x-ray-diffraction techniques. Because the x-ray beam size is large compared with the crystallite dimensions of highly oriented pyrolytic graphite (HOPG, the material used for most properties measurements),[19] complete structural determinations for samples based on HOPG are difficult with the x-ray technique. In the case of electron diffraction, a beam size of 1-μm diameter can be routinely achieved. Since this beam size is comparable with crystallite dimensions in HOPG,[19] electron diffraction offers significant advantages for detailed structural analysis of samples based on HOPG.

The electron-diffraction technique, however, has several aspects that deserve further comment. To obtain a good diffraction pattern, it is necessary for the electrons to penetrate a number of crystal planes. For this reason electron energies in the 50–100-keV range are selected. The penetration depth for such a beam is ≈ 1000 Å, and therefore, thin samples must be prepared. In the case of graphite intercalation compounds, such thin samples can be made by cleavage perpendicular to the c direction, utilizing the low interplanar binding in this direction. Because of the general impenetrability of electrons to condensed matter, electron-diffraction measurements cannot be made through the encapsulating glass or quartz ampoules that normally surround the intercalated graphite samples to prevent intercalate desorption. Thus special handling techniques must be developed for the preparation and mounting of the samples in the transmission electron microscope where the electron-diffraction measurements are carried out. These special handling techniques involve preparation of thin samples with the properties of the bulk material, without intercalate

desorption or the introduction of strains.

Electron diffraction differs from other diffraction techniques because of the importance of multiple-diffraction effects.[20] If the graphite and intercalate layers are commensurate, and if the electron beam is in the c direction, no new diffraction spots will appear. However, in this case, the relative spot intensities of unequivalent spots will differ from calculations based on structure factors because of multiple-diffraction effects. On the other hand, when the graphite and intercalate layers are incommensurate, multiple diffraction gives rise to extremely complex superlattice patterns. For such incommensurate lattices, the x-ray-diffraction patterns are simpler because of the absence of multiple-diffraction effects. Nevertheless, because of the large x-ray beam size relative to the crystallite domain size of HOPG, the x-ray-diffraction patterns are not single-crystal patterns but rather powder patterns. By comparing single-crystal x-ray-diffraction patterns with the corresponding electron-diffraction patterns, we can identify diffraction spots that are associated with multiple-diffraction effects. The identification of the primary diffraction pattern is necessary if information about the intercalate ordering is to be obtained.

The x-ray- and electron-diffraction techniques are also complementary because of differences in the wavelength of typical electron and x-ray beams. In order to have sufficient bulk penetration, electron-beam energies are typically 50–100 keV, resulting in a very small electron wavelength $\lambda = 0.038$ Å for a 100-keV electron and thus a very large Ewald diffraction sphere. For the electron-diffraction patterns reported in this work, the Ewald sphere can be approximated by a plane in reciprocal space which for electrons incident along the c axis becomes coincident with the $l=0$ reciprocal-lattice plane. This situation is in contrast with the case of x-ray diffraction where the Laue condition is satisfied for points on different planes in reciprocal space. In this sense, the two techniques sample a somewhat different collection of points in reciprocal space.

Graphite-rubidium was chosen as the material for the present study because of the relative ease of sample preparation and because of the availability of information on this material from previous studies using x-ray-diffraction,[10,16,21] electron-diffraction,[22,23] and neutron-diffraction[15] techniques. Figure 1(a) shows the structure proposed by Rüdorff and Schulze[16] for first-stage alkali-metal compounds of the C_8X form, and subsequently confirmed by Nixon and Parry[8] based on a single-crystal host material. The work of Nixon and Parry further showed C_8K and C_8Rb to have

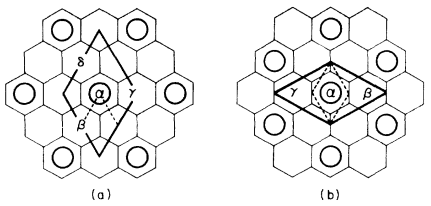

FIG. 1. At the corners of each hexagon is a carbon atom in each of the graphite layers. Dark lines denote the real-space unit cell for the superlattice structures and the dashed lines denote the graphite unit cell. The α intercalant (large circles) layer is shown projected onto a graphite layer. (a) The superlattice structure is $p(2\times2)R\,0°$, and sequential intercalate layers have occupation on $\alpha,\beta,\gamma,\delta$ sites. (b) The superlattice structure is $p(\sqrt{3}\times\sqrt{3})R\,30°$, and sequential intercalate layers have occupation on α,β,γ sites. For this structure the basis vectors for the superlattice are rotated by 30° relative to those for graphite.

the stacking sequence $\alpha,\beta,\gamma,\delta$ indicated in Fig. 1 but C_8Cs to have a different stacking sequence α,β,γ.[21] Electron-diffraction measurements by Halpin and Jenkins[13] on a saturated graphite-potassium sample (which they identified as C_8K) showed only the graphite electron-diffraction pattern. They further showed that by intercalate desorption, superlattice spots could be introduced either by the presence of imperfections in the bulk[7] or by growth of an epitaxial film.[13] These and other superlattice structures were subsequently reported by Chung[22,23] in compounds with K, Rb, and Cs. In the work of Chung *et al.*,[22,23] the simple graphite pattern indicative of $\alpha,\beta,\gamma,\delta$ stacking was not reported.

Of particular relevance to the present work is the elastic-neutron-scattering study by Ellenson *et al.* on C_8Cs and C_8Rb based on HOPG host materials.[15] In the case of C_8Cs, they observed the α,β,γ stacking sequence for temperatures $4<T<300$ K, thereby showing that the previous x-ray-diffraction results[7] were also applicable to compounds based on an HOPG host material. The neutron-diffraction experiments on C_8Rb, however, produced different c-axis stacking patterns depending on the temperature range and on previous sample treatment.[15] Upon annealing the materials at 747 K for two days, a diffraction pattern characteristic of the $\alpha,\beta,\gamma,\delta$ stacking of successive Rb layers was observed at room temperature, while at higher temperatures (721 K) a well-ordered phase with α,β stacking was reported.[15] On the other hand, the pattern from an as-grown C_8Rb sample without the high-temperature anneal did not exhibit a diffraction pattern associated with any definite intercalate layer stacking. This work is of great significance in pointing out the need for annealing stage-1 samples based on HOPG host

materials for quantitative measurements where in-plane structural order is important.

Electron diffraction provides a powerful tool for the identification of certain interplanar stacking orderings. In particular, the $\alpha,\beta,\gamma,\delta$ stacking of Fig. 1(a) results in a vanishing of the superlattice reflections. This can be understood by consideration of the structure factor

$$F_{hkl} = \sum_{j=\alpha}^{\delta} f_{\mathrm{Rb}} \exp[-2\pi i(hu_j + kv_j + lw_j)] , \qquad (1)$$

where f_{Rb} is the atomic scattering amplitude for Rb and the sum on j is taken over the four layers $j=\alpha,\beta,\gamma,\delta$. The C_8X unit cell of Fig. 1(a) is denoted by the superlattice notation $p(2\times2)R\,0°$, where p denotes a primitive hexagonal unit cell and the (2×2) corresponds to an in-plane area that is four times greater than that for graphite. The in-plane unit vectors $\hat{a}_1^{(2)}$ and $\hat{a}_2^{(2)}$ for the superlattice are parallel to the graphite unit vectors $\hat{a}_1^{(1)}$ and $\hat{a}_2^{(1)}$ (0° rotation) and given by

$$\begin{aligned} \hat{a}_1^{(2)} &= a_o(\sqrt{3}\,, 1, 0) = 2\hat{a}_1^{(1)} , \\ \hat{a}_2^{(2)} &= a_o(-\sqrt{3}\,, 1, 0) = 2\hat{a}_2^{(1)} , \\ \hat{c}_1^{(\alpha\beta\gamma\delta)} &= c_x(0, 0, 8) = 4\hat{c}_1^{(1)} , \end{aligned} \qquad (2)$$

where $a_1^{(1)}$, $a_2^{(1)}$, and a_o are, respectively, the basis vectors and lattice constant for pure graphite and $2c_x$ is the distance between two adjacent intercalate layers. For the $\alpha,\beta,\gamma,\delta$ stacking sequence, the position vectors for the intercalate are written $(u_j\hat{a}_1^{(2)}, v_j\hat{a}_2^{(2)}, w_j\hat{c}_1^{(\alpha\beta\gamma\delta)})$, where the (u_j, v_j, w_j) parameters on each of the layers are

$$\begin{aligned} &(\tfrac{1}{2}, \tfrac{1}{2}, -\tfrac{1}{8}) \quad j=\alpha , \\ &(\tfrac{1}{2}, 1, \tfrac{1}{8}) \quad j=\beta , \\ &(0, 0, \tfrac{3}{8}) \quad j=\gamma , \\ &(1, \tfrac{1}{2}, \tfrac{5}{8}) \quad j=\delta . \end{aligned} \qquad (3)$$

Substitution of the (u_j, v_j, w_j) vectors of Eq. (3) into the structure factor of Eq. (1) yields zero except for $(h, k, 0)$ values corresponding to the graphite host lattice. Thus for the $\alpha,\beta,\gamma,\delta$ interplanar ordering, the intercalate and graphite diffraction patterns are *coincident*. A similar analysis applies to the α,β,γ interplanar intercalate stacking for the C_6X structure of Fig. 1(b) which characterizes C_6Li at low temperatures,[18] and has a $p(\sqrt{3}\times\sqrt{3})R\,30°$ superlattice structure, with an in-plane area three times greater than that for graphite and unit vectors rotated by 30° from those of graphite.

At present the structure of the high-stage ($n \geq 2$) alkali-metal compounds is not well established. In particular, since no definitive structural model for the in-plane ordering has been proposed for these

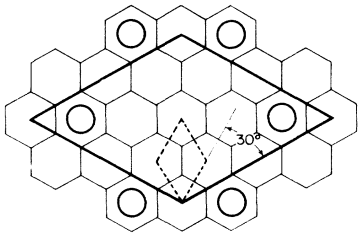

FIG. 2. At the corners of each hexagon in a graphite layer is a carbon atom. Dark lines denote the real-space unit cell for the superlattice structure $h(\sqrt{12}\times\sqrt{12})R\,30°$, and the dashed lines denote the graphite unit cell. The intercalant occupation (large circles) for a typical intercalate layer is shown projected onto the graphite layer. We note that there are 12 equivalent intercalant site occupations. The superlattice structure is of the honeycomb (h) type, and the basis vectors for the superlattice are rotated by 30° relative to those for graphite.

compounds consistent with experimental results, a simple Rüdorff-Schulze model[16] with the $C_{24}X_2$ in-plane ordering shown in Fig. 2 has been commonly used. The Rüdorff-Schulze model denoted by the superlattice structure $h(\sqrt{12}\times\sqrt{12})R\,30°$ (h denotes honeycomb arrangement) was originally motivated by matching the chemical analysis of weight uptake of the intercalated alkali metals to the x-ray-diffraction results for staging.

Subsequently, detailed x-ray-diffraction studies of $(hk0)$ reflections by Parry *et al.*[7-10] did not confirm the Rüdorff-Schulze in-plane structure of Fig. 2. Their work [8-10] on the stacking sequences of the graphite and intercalate layers for stage $n=2$ K, Rb, Cs compounds was also not in agreement with that of Rüdorff and Schulze, who reported stacking sequences for high-stage $2 \leq n \leq 5$ compounds.

The low-temperature stacking sequences were identified[21] as $A\alpha AB\beta BC\gamma CA\alpha'AB\beta'BC\gamma'C$ for a stage $n=2$ K compound, $A\alpha AB\beta BC\gamma C$ for stage $n=2$ Rb and Cs compounds, where capital Latin letters denote the graphite layers and Greek letters the intercalate layers. At low temperatures, the intercalate layers exhibit in-plane order which disappears above the order-disorder transition temperature (98 K for stage-2 graphite-K).[9, 10] Parry *et al.* reported that the disordered phase (associated with a streak diffraction pattern) was maintained up to room temperature. Similar phenomena were later reported by other authors[24, 25] using x-ray-diffraction techniques. Parry himself[7] interpreted the streaks to indicate a preferred orientation, the two nearest-neighbor intercalate sites possessing a preferred orientation but with random registration of each site.

Parry subsequently attempted[7] to determine the

low-temperature in-plane ordering for high-stage $2 \leq n \leq 5$ Cs compounds using x-ray-diffraction techniques and suggested the presence of the following stage-dependent structures: for $n = 2$ an in-plane $p(2 \times 2)R\,0^\circ$ structure, for $2 \leq n \leq 4$ a mixture of coexisting phases with $o(3 \times \sqrt{7})$ and $o(\sqrt{39} \times \sqrt{39})$ structure (o denotes oblique), and for $n = 5$ an in-plane $p(\sqrt{7} \times \sqrt{7})R\,19.1^\circ$ structure. Parry's argument, however, in terms of an intercalate site occupancy probability, failed to provide a definitive and consistent low-temperature in-plane structure for the high-stage Cs compounds.

In this paper we give evidence for a commensurate low-temperature in-plane ordering for stage $n = 2$ Rb compounds, based on the electron-diffraction patterns. It is significant that the observed low-temperature in-plane ordering differs from the proposed Rüdorff-Schulze $h(\sqrt{12} \times \sqrt{12})R\,30^\circ$ structure. We also describe at higher temperatures a phase transition between two ordered states. At the same transition temperature, previous workers using x-ray-diffraction and electrical-conductivity measurements have interpreted this transition as an order-disorder phase transition.[9,10,25,26] The present identification of this structural phase transition exploits the small electron-beam size and short wavelength of the incident electron beam in our experimental system.

II. EXPERIMENTAL DETAILS

Electron-diffraction observations were made through the c face of thin samples, using a Philips EM300 transmission electron microscope with a typical electron energy of 100 kV and a beam size less than 1 μm. Such electrons can only be transmitted through specimens of less than 1000-Å thickness. The electron beam was directed along the c axis of the sample, so that the measurements are primarily sensitive to the in-plane ordering of the graphite and intercalate layers, and the correlation between their ordering.

Relatively large bulk samples ($\approx 6 \times 8 \times 0.5$ mm^3) were prepared by the two-zone method,[8] in which careful regulation of the temperature of the two zones is required. The large bulk samples were prepared in a rectangular-shaped pyrex tubing (glass ampoule), which was initially evacuated. X-ray-diffraction measurements using an Mo x-ray tube were made through the glass ampoule to verify that the material was single stage and to determine its stage index. Some electron-diffraction patterns were taken on specimens prepared from this as-grown material. Electron-diffraction patterns were also taken on samples prepared from a material that was annealed in the glass ampoule for two days at 730 K. The x-ray-diffractometer traces for the annealed materials yielded the same stage index as the corresponding as-grown materials. The bright-field microstructure image of the sample through the transmission electron microscope showed that the annealing process has a major effect on improving the sample homogeneity. These findings are consistent with results reported by Ellenson *et al.* using the neutron-diffraction technique.[15]

To prepare the thin samples (<1000 Å) needed for the transmission-electron-microscopy study and to reduce the possibilities of sample oxidation, hydration, or intercalate desorption, the following sample-handling technique was adopted. First, the well-characterized as-grown or annealed material, still in the original glass ampoule, was placed in a dry box. The dry box was first purged with an argon-H_2 gas mixture and was then passed through an impurity gas absorber before the glass ampoule was cracked in the dry box. A thin sample was prepared by cleavage from the bulk material. The thin sample was then mounted in the dry box on the copper-rhodium or nickel grid of the electron-microscope sample holder. The sample holder containing the mounted sample was carefully transferred from the dry box to the electron-microscope sample goniometer stand, which was air locked. Once introduced into the vacuum of the electron-microscope column, the sample assembly was then rapidly cooled down to 110 K with liquid nitrogen. With practice, the entire process from the breaking of the glass ampoule to the cooling of the sample holder could be carried out in five min. For stage-1 C_8Rb the sample surface had a golden color through a conventional optical microscope before and after the electron-diffraction measurements, thereby giving evidence that the sample remained stage 1 during the experiments. The adequacy of the sample-handling technique could be examined not only by the sample's color but also by the diffraction patterns themselves. Good sample-handling techniques were critical to the success of the experiment.

Significant intercalate desorption occurred near the sample edges except at the lowest temperatures. The desorption rate increases with increasing temperature. The electron-diffraction patterns themselves can be used to provide information on the degree of intercalate desorption from the sample edge.

Prior to taking an electron-diffraction picture, suitably thin regions of the sample are selected from the bright-field microstructure image on the (fluorescent) screen. Electron-diffraction patterns are taken as a function of temperature on the same region of the sample. In these experiments both cooling and heating sample holders were available,

allowing measurements to be made in the temperature range $110 < T < 900$ K. At a given temperature, we verified that the observed pattern was independent of the region on the sample selected for observation. The best resolution of the electron-diffraction spots was obtained in regions where the sample was relatively thin.

Bright-field image micrographs with magnifications from 27 000 to 205 000 have also been taken with the Philips EM300 for the same regions on the sample where the electron-diffraction pattern was measured, initially to verify the homogeneity of the sample and later to study the change in the real image at phase transitions. The simultaneous observation of a real image and an electron-diffraction pattern turned out to be significant for the study of temperature-dependent effects.

III. RESULTS AND DISCUSSION

The diffraction pattern obtained for stage-1 annealed C_8Rb for $110 < T < 300$ K is a simple graphite pattern, as shown in Fig. 3(a). Also presented [see Fig. 3(b)] is a schematic representation of this pattern.[27] This result, showing the intercalate layers to give rise to a diffraction pattern identical with the graphite host, is consistent with previous work by Halpin and Jenkins[13] on C_8K and with the structure factor computed from the atom site locations for $\alpha, \beta, \gamma, \delta$ interlayer stacking given in Sec. I and shown in Fig. 1(a).

This is the first reported observation of the simple graphite pattern for annealed C_8Rb using the electron-diffraction technique, giving results below 300 K that are in agreement with x-ray-diffraction[16] and neutron-diffraction[15] measurements. This agreement is interpreted as providing evidence for the reliability of our sample-handling techniques.

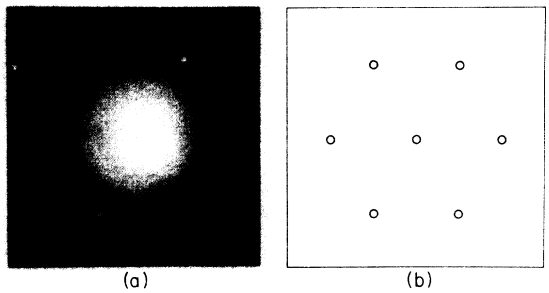

FIG. 3. (a) In-plane electron diffraction pattern for a well annealed stage-1 graphite-Rb (C_8Rb) sample for $T \lesssim 300$ K. (b) A schematic representation of the diffraction pattern in (a). The open circles denote the graphite pattern. The absence of a superlattice pattern indicates that the diffraction pattern for the intercalate is coincident with that for the graphite. This diffraction pattern is consistent with the sequential $\alpha, \beta, \gamma, \delta$ intercalate layer stacking of Fig. 1(a) and the sequential α, β, γ intercalate layer stacking of Fig. 1(b).

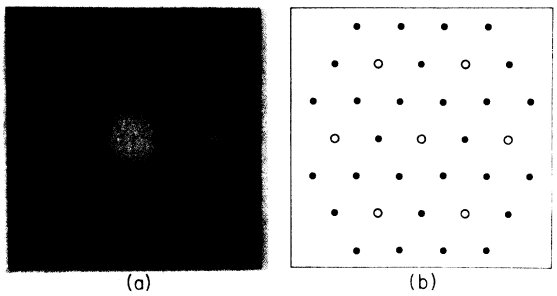

FIG. 4. (a) In-plane electron diffraction pattern for an as-grown stage-1 graphite-Rb (C_8Rb) sample and also for a well annealed stage-1 graphite-Rb (C_8Rb) sample for $T \gtrsim 300$ K. (b) A schematic representation of the diffraction pattern in (a). The superlattice structure indicated by the closed circles is consistent with a random arrangement of intercalate layers each having either α, β, γ, or δ site occupations.

The simple diffraction pattern of Fig. 3(a) is preserved upon temperature cycling in the range $110 < T < 300$ K. If a well annealed stage-1 graphite-Rb sample is heated into the temperature range $300 < T < 330 \pm 10$ K, the superlattice diffraction pattern of Fig. 4(a) is observed. The superlattice spots marked by solid circles in the schematic diagram of Fig. 4(b) are located at the midpoint between two adjacent graphite spots, corresponding to a $p(2\times2)R\,0°$ superlattice pattern and identified with the absence of the $\alpha, \beta, \gamma, \delta$ intercalate interplanar stacking sequence. Without the $\alpha, \beta, \gamma, \delta$ stacking order, the structure factor for the superlattice $(h, k, 0)$ reflections no longer vanishes upon summation over the intercalate layers. The superlattice diffraction pattern of Fig. 4(a) can arise from the *random* stacking of $p(2\times2)R\,0°$ commensurate intercalate structures, or from ordered stacking sequences such as the $\alpha\beta, \alpha\beta\gamma$, and $\alpha\alpha$ ordered arrangements. If the sample temperature is subsequently lowered below 300 K, the simple diffraction pattern of Fig. 3(a) is recovered. Thus the transition between the superlattice pattern of Fig. 4(a) and the graphite pattern of Fig. 3(a) is reversible for a well annealed stage-1 graphite-Rb sample provided that the temperature is not raised above 330 ± 10 K within the electron-microscope column which is in vacuum.

The diffraction patterns for the unannealed as-grown stage-1 C_8Rb samples (grown from an HOPG host) always show a superlattice structure such as Fig. 4(a) in the temperature region $110 < T < 320$ K. Unlike the case of well annealed C_8Rb, the simple graphite pattern of Fig. 3(a) is never observed. Observation of the real-image micrograph at ~110 K using the electron microscope shows that the

Rb layers of the well annealed C_8Rb are more homogeneous than those of the as-grown C_8Rb samples. The formation of clusters, which is described in relation to diffraction results later in this section, was less evident at 110 K for the well annealed than for the as-grown stage-1 graphite-Rb samples. Thus the annealing process provides increased sample homogeneity and higher structural order for the first-stage graphite-Rb compounds, while the as-grown samples lack $\alpha, \beta, \gamma, \delta$ intercalate stacking order.

Electron-diffraction measurements also have been carried out at temperatures up to 900 K for both well annealed and as-grown stage-1 Rb compounds. As the temperature is increased above 300 K, desorption becomes significant after several minutes, causing changes in the electron-diffraction pattern shown in Fig. 4(a). These changes include a decrease in the intensity of the superlattice diffraction spots, the formation of straight lines joining second-neighbor graphite spots, and the appearance of additional diffraction spots. Since the desorption rate increases with increasing temperature, the changes in the diffraction pattern become more marked as the temperature is increased. The changes are irreversible, and the pattern of Fig. 4(a) does not return after the sample temperature is lowered to room temperature. The behavior of desorbed as-grown and well annealed stage-1 graphite-Rb samples is similar.

A totally different superlattice pattern than described above is found at low temperatures, $T < 200$ K, for the higher-stage graphite-Rb compounds. This superlattice pattern is shown in Fig. 5(a) for a stage $n = 2$ compound at $T = 120$ K and a schematic representation of this diffraction pattern is shown in Fig. 5(b). Around each of the graphite spots in this figure are twelve superlattice spots giving rise to a pair of hexagonal superlattices. One hexagonal superlattice is rotated by $+19.1°$ with respect to the graphite unit cell, while the other superlattice is rotated by $-19.1°$. In the schematic diagram, the innermost pair of hexagons around a central graphite spot can be interpreted as the first-order pattern, and the other spots are indexed as higher-order diffraction spots. The intensity of the diffraction spots decreases monotonically as the spot index increases, i.e., as the distance from the central spot increases. The direct lattice corresponding to the diffraction pattern in Fig. 5(b) is shown in Fig. 6 in which the small carbon atoms in a graphite layer reside at the corners of the hexagonal network, while the large Rb ions (ionic radius = 1.48 Å) on the intercalate layer (marked by speckled circles) project onto the center of the hexagonal network. This arrangement minimizes the free energy of the

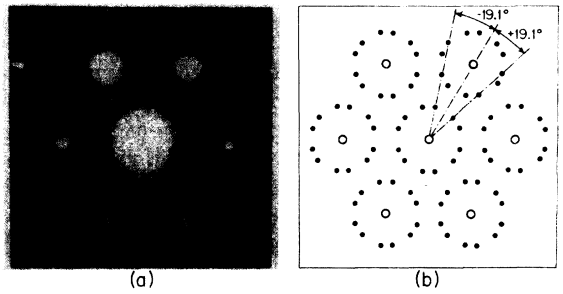

FIG. 5. (a) Low-temperature ($T < 170$ K) in-plane electron-diffraction pattern for graphite-Rb sample of stage $n = 2$. Similar patterns have been observed at low temperatures for samples with stages $n = 3, 4, 7$. (b) A schematic representation of the diffraction pattern in (a). This diffraction pattern shows two hexagonal superlattices rotated by $\pm 19.1°$ relative to the graphite lattice, and commensurate with the graphite lattice.

system. The Rb ions form a $p(\sqrt{7} \times \sqrt{7})R\,19.1°$ superlattice structure that is commensurate relative to the graphite unit cell. The other superlattice structure in Fig. 5(b) corresponds to a similar in-plane ordering but with a rotation angle of $-19.1°$ rather than $+19.1°$. We interpret these results to indicate that some parts of the sample exhibit the $+19.1°$ rotation, and other parts the $-19.1°$ rotation. The dark lines in Fig. 6 denote a commensurate in-plane unit cell in which 14 carbon atoms and one Rb ion are included. Also shown in the figure is the graphite unit cell. The in-plane real lattice constant for the large unit cell is 6.51 Å which equals $\sqrt{7}a_0$ (where $a_0 = 2.46$ Å is the graphite in-plane lattice constant). This in-plane structure pertains to an in-plane stoichiometry $C_{14}Rb$. In this paper we use the abbreviated $C_{14}X$ notation

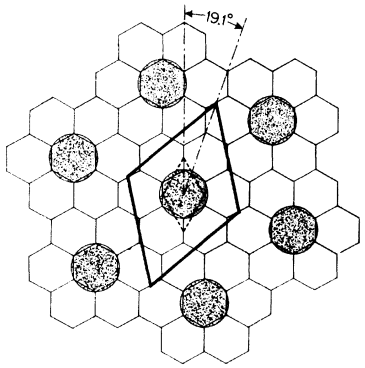

FIG. 6. Real-space superlattice structure corresponding to the $+19.1°$ reciprocal lattice structure of Fig. 5(b). The large shaded circles denote the superimposed Rb ions and the dark lines the $p(\sqrt{7} \times \sqrt{7})R\,19.1°$ superlattice, which is commensurate with the graphite structure (unit cell indicated by dashed lines). In the unit cell are 14 carbon atoms for each Rb ion.

to denote the unit cell $p(\sqrt{7}\times\sqrt{7})R\,19.1^\circ$ of Fig. 6.

We identify for the first time the $C_{14}X$ structure as the low-temperature in-plane ordering for stage $n=2$, 3, 4, and 7 graphite-Rb compounds. Parry suggested a similar structure for a stage $n=5$ Cs compound using the x-ray-diffraction technique.[7] We have also observed the $C_{14}X$ structure for Cs and K compounds at low temperature using electron diffraction, and these results will be reported elsewhere.

The $C_{14}X$ in-plane ordering is observed for compounds with $n\geq 2$ below a certain temperature denoted by T_U. Although the dependence of T_U on stage index n has not been fully established, it is found that T_U decreases with increasing n. For example, the stage $n=2$ Rb compound exhibits the $C_{14}X$ in-plane ordering below 170 K, corresponding to a broad anomaly observed in the electrical conductivity,[26] while for a stage $n=3$ Rb compound, T_U occurs at about 140 K.

In a temperature range of 20 to 30 K about T_U, a reversible structural transition occurs from the $C_{14}X$ in-plane ordering to a distinctly different in-plane ordering denoted by $C_\nabla X$. Figure 7(a) shows an electron-diffraction pattern for a stage-2 Rb compound that is characteristic of the temperature regime $T>T_U$. The corresponding schematic diagram is illustrated in Fig. 7(b), where the larger dark circles denote superlattice diffraction spots of higher intensity relative to the smaller dark circles. The $C_\nabla X$ structure commonly appears above T_U for stage $2\leq n\leq 7$ Rb compounds as well as for high-stage ($n\geq 2$) Cs compounds. Although a real-space lattice structure corresponding to the superlattice diffraction pattern shown in Fig. 7(a) has not yet been completely analyzed because of its complexity, our preliminary analysis based on a comparison of observed diffraction patterns

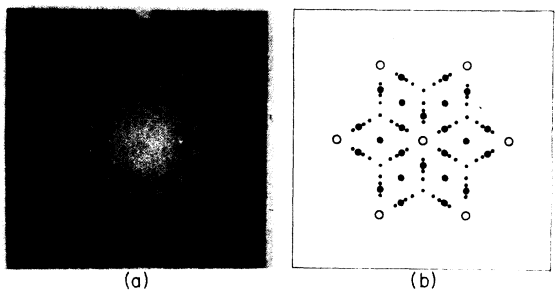

FIG. 7. (a) High-temperature ($170<T<620$ K) in-plane electron-diffraction pattern for stage-2 graphite-Rb samples (and referred to by $C_\nabla X$ in the text). Similar patterns are observed for samples with stages $n=3,4,7$. (b) A schematic representation of the diffraction pattern in (a). The open circles refer to the graphite pattern, the large solid circles to intense superlattice spots, and the small circles to weak superlattice spots.

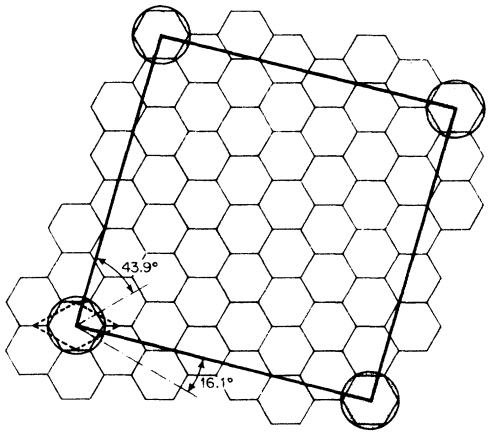

FIG. 8. In-plane ordering in real space of the $o(\sqrt{39}\times\sqrt{39})R(16.1^\circ, 43.9^\circ)$ commensurate superlattice. The dark lines show the unit cell containing 90 carbon atoms and one Rb ion. The figure shows the 16.1° and 43.9° angles of rotation of the basis vectors relative to those of the graphite unit cell (dashed lines).

to patterns calculated on the basis of various reciprocal lattices suggests that the in-plane superlattice could be related to a superposition of $h(\sqrt{12}\times\sqrt{12})R\,30^\circ$ and $o(\sqrt{39}\times\sqrt{39})R(16.1^\circ, 43.9^\circ)$ (Ref. 28) superlattices where the honeycomb $h(\sqrt{12}\times\sqrt{12})R\,30^\circ$ is the one proposed by Rüdorff and Schulze[16] for $n\geq 2$ (see Fig. 2), and the $o(\sqrt{39}\times\sqrt{39})R(16.1^\circ, 43.9^\circ)$ superlattice is shown in Fig. 8. For the calculated diffraction patterns, we assumed that the superlattice was commensurate to the graphite lattice and that the alkali-metal ions were separated from one another at a distance between two and five times the graphite lattice constant a_0 because of the relatively large size of the alkali-metal ions. The superposition of the calculated diffraction patterns is shown in Fig. 9 demonstrating the fit of this structural model to the observed pattern. In Fig. 9 the $h(\sqrt{12}\times\sqrt{12})R\,30^\circ$ superlattice is represented by open circles and the $o(\sqrt{39}\times\sqrt{39})R(16.1^\circ, 43.9^\circ)$ superlattice by solid triangles and small solid circles, and it is seen that some of the observed spots are unidentified (marked by small open circles), while some of the calculated spots are not found in the observed pattern (marked by small solid circles). One should note that the above-mentioned combination of two superlattices is not unique. We note that different real-space superlattices can in some cases yield identical in-plane diffraction patterns, for example, the $h(\sqrt{12}\times\sqrt{12})R\,30^\circ$ and $o(\sqrt{3}\times 3)R(30^\circ, 60^\circ)$ superlattices yield the same diffraction patterns. An ordered array of *unoccupied* sites (vacancies[29]) in some close-packed superlattices can also give rise to a complicated though ordered diffraction

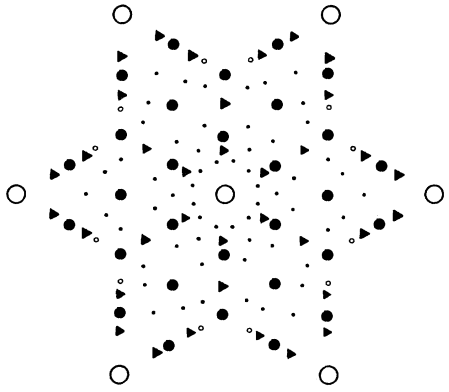

FIG. 9. Match of the $h(\sqrt{12}\times\sqrt{12})R\,30°$ (solid •) and the $o(\sqrt{39}\times\sqrt{39})R(16.1°, 43.9°)$ (solid ▲ and small solid •) superlattices to the $C_{\nabla}X$ structure. The small solid • denote extra spots in the $o(\sqrt{39}\times\sqrt{39})R(16.1°, 43.9°)$ structure that do not appear in the electron-diffraction pattern for the $C_{\nabla}X$. The spots of $C_{\nabla}X$ that are not matched by these two superlattices are indicated by a small open ◦.

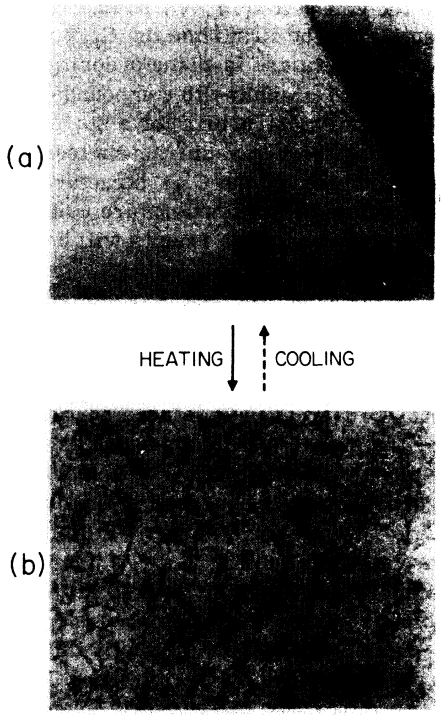

FIG. 10. (a) Bright-field image for a stage-2 graphite-Rb compound taken at 110 K. This micrograph is typical of low-temperature electron micrographs taken for $T<T_0\simeq T_U$ ($T_0=160$ K and $T_U=170$ K). We identify the dark areas with small clusters of ~40-Å diameter. (b) Bright-field image taken on the same spot of the sample as in (a), but at $T=223$ K ($>T_U$). Larger clusters of ~180-Å diameter and channels are found for micrographs above T_U. A reversible variation in the cluster size between (a) and (b) is indicated by both straight and broken arrows, respectively, denoting heating and cooling processes.

pattern.[7] The structure associated with $o(\sqrt{39}\times\sqrt{39})R(16.1°, 43.9°)$ might be this kind of superlattice. Until now, our analysis has not yielded a single-phase ordering for the $C_{\nabla}X$ electron diffraction pattern shown in Fig. 7(a), suggesting that several alkali-metal domains with different lattice structures might coexist within the intercalate layers. The coexistence of dense commensurate structures with effectively vacant regions is commonly observed in adsorption studies on the basal graphite surface.[30]

The observation of the $C_{\nabla}X$ pattern requires the reexamination of previous structural models[7,9,10] in which a disordered phase was reported in a temperature region, e.g., $159<T<360$ K[10,26] for a stage-2 Rb compound based on x-ray diffraction measurements. With the electron-diffraction technique, we observe for stage-2 graphite-Rb an *ordered* phase $C_{\nabla}X$ (rather than a disordered phase) at temperature $170<T\lesssim 620$ K. Since we use a small electron beam size ~1 μm, we are able to probe a single-crystal domain of compounds based on pyrolytic graphite (HOPG) host materials.[19] In contrast, the information available by x-ray- and neutron-diffraction measurements on similar samples is spatially averaged over multiple domains. This may account for the qualitative discrepancy between previous results[10] and our electron-diffraction results.

One notes that the $C_{\nabla}X$ in-plane ordering may be more closely packed than the $C_{14}X$, which suggests that the in-plane structure is more condensed at high temperatures than at low temperatures. Such an unexpected result might be related to our real-image observations in these compounds. By taking electron micrographs in the imaging mode of the electron microscope, we have observed the temperature dependence of the real-image patterns as a function of temperature with particular reference to the phase transition between the ordered $C_{14}X$ and $C_{\nabla}X$ structures.

Typical real images obtained for a stage-2 Rb compound are shown in Fig. 10(a) at $T=110$ K for the $C_{14}X$ structure and in Fig. 10(b) at $T=223$ K for the $C_{\nabla}X$ structure. In both pictures the dark part of the micrograph is tentatively identified with clusters,[31] and the bright part with graphite, because of the larger electron scattering amplitude for Rb than for graphite. The micrograph in Fig. 10(a) taken at 110 K displays small clusters, typically of ~40-Å diameter, and a growth pattern similar to that observed in the growth process of thin metallic films. Because of the resolution limitation of this microscope, particles of less than

10-Å diameter cannot be resolved. As the temperature is increased, the density of clusters increases, whereas the cluster size remains almost unchanged up to the temperature T_0 ($\simeq T_U$) where a drastic change in cluster size is observed, changing from ~40 Å for $T \lesssim T_0$ to ~180 Å diameter for $T \gtrsim T_0$. Figure 10(b) shows the real-space image taken on the same spot of the stage-2 Rb sample as Fig. 10(a) but at a temperature of 223 K which is above $T_0 \cong 160$ K. For $T \gtrsim T_0$, the Rb clusters coalesce forming larger clusters or channels. During the experimental run, the image of Fig. 10(b) did not show any significant change until 620 K, which corresponds to the transition temperature T_m to a high-temperature phase in the intercalate layer[32,33] as discussed below.

On cooling, the large clusters decrease in size, and at a critical temperature T_0' a dramatic change in cluster size to the image shown in Fig. 10(a) occurs. Only when the temperature cycling is carried out quickly enough so that significant Rb desorption is avoided (e.g., at a rate of 100 K/min), the thermal hysteresis ($T_0 - T_0'$) is found to be small (~10 K). The solid (heating) and broken (cooling) arrows between Figs. 10(a) and 10(b) indicate that the variation in the Rb cluster size is reversible on thermal cycling (heating and cooling through T_U) provided that intercalate desorption effects are minimized. It is reasonable that desorption gives rise to hysteresis effects since T_U is observed to decrease with increasing stage. The clustering phenomenon is illustrated more quantitatively in Fig. 11, where three axes are shown for a stage-2 graphite-Rb sample: the density of clusters in arbitrary units, the temperature in K, and the cluster size in Å. Of significance is the rapid change in cluster size for $T \sim T_0 = 160$ K which is close to T_U (170 K) for this compound. A lower limit to the temperature for cluster formation could not be obtained because the lowest achievable temperature of our electron microscope was ~110 K. A detailed report on the observation of the real-space images for other alkali-metal intercalants as a function of temperature and

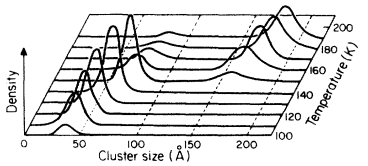

FIG. 11. Qualitative three-dimensional plot showing the relation between the density of clusters, temperature, and cluster size for a stage-2 graphite-Rb sample. Note the dramatic change in cluster size in a narrow temperature range near T_U.

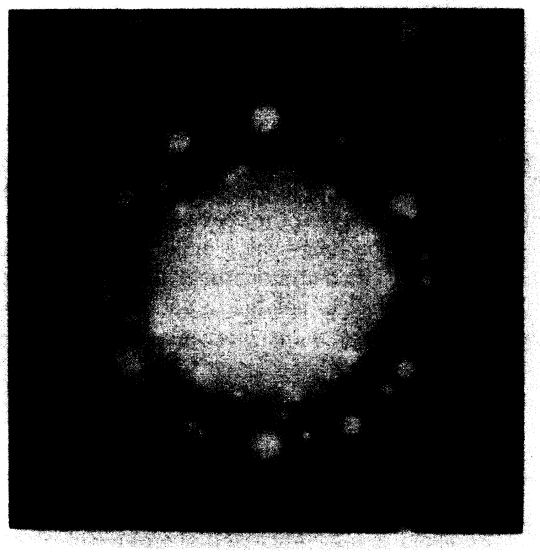

FIG. 12. Electron-diffraction pattern taken on a stage-2 Rb compound at 659 K, showing a very complicated intercalate arrangement. The multitude of diffraction spots and the bright halo are both associated with scattering by the intercalant. The graphite spots are undisturbed, but difficult to distinguish from the background.

stage will be presented elsewhere.

At yet higher temperatures, stage-2 Rb and Cs compounds, furthermore, exhibit a structural transformation from the ordered $C_\nabla X$ structure to a multiphase intercalate layer above a transition temperature T_m, as shown in Fig. 12. This transition is fully reversible and no significant thermal hysteresis has been observed provided that there is no significant intercalate desorption; to avoid intercalate desorption, a rapid heating and cooling rate of ~100 K/min was chosen. On the basis of the observed structural transformation in the electron-diffraction patterns, we obtain $T_m = 620$ K for a stage-2 Rb compound, and $T_m = 625$ K for a stage-2 Cs compound. The complicated spot pattern shown in Fig. 12 could be due to the coexistence of many ordered phases. A quantitative study of the spot pattern of Fig. 12 is difficult because of the bright background that covers the entire picture plate and makes the identification of even the graphite diffraction spots difficult. Previous workers using x-ray and neutron diffraction have observed structural phase transitions in the same temperature region, but these workers have identified the phase transition with a melting of the intercalate layer. For example, neutron-diffraction measurements for a stage-1 graphite-Rb compound[15] showed a phase transition at $T_m = 747$ K, while x-ray-diffraction measurements for stage-1 and desorbed stage-1 graphite-Cs compounds yielded

$T_m = 608$ K (on heating). Whereas our results yield values for the transition temperature similar to those obtained with x-ray- and neutron-diffraction techniques, it would seem that melting to a two-dimensional lattice gas, where the $\alpha, \beta, \gamma, \delta$ sites of Fig. 1(a) would be occupied with equal probability, should give a simple graphitic diffraction pattern. The observation of a spot pattern (Fig. 12) gives evidence for long-range order, which is not consistent with a two-dimensional liquid or lattice gas. Further work is needed to establish conclusively the structure of the intercalate layer above T_m.

IV. SUMMARY

In this paper electron-diffraction results are reported in the temperature range $110 < T < 900$ K for graphite-Rb intercalation compounds based on HOPG host material. Annealed stage-1 samples show the simple graphite pattern below ~300 K, corresponding to a $p(2\times2)R\,0°$ in-plane intercalate ordering with $\alpha, \beta, \gamma, \delta$ interlayer intercalate stacking order. Above ~300 K, a superlattice diffraction pattern is observed, corresponding to the $p(2\times2)R\,0°$ in-plane ordering, but lacking the $\alpha, \beta, \gamma, \delta$ interlayer intercalate stacking. At yet higher temperatures, intercalate desorption occurs giving rise to irreversible behavior. If intercalate desorption is prevented, the transition at ~300 K between the two ordered structures is fully reversible. An unannealed as-grown stage-1 graphite-Rb sample does not exhibit the $\alpha, \beta, \gamma, \delta$ stacking in the temperature range $110 < T < 320$ K.

For the higher-stage graphite-Rb compounds ($n = 2, 3, 4, 7$), the low-temperature $110 < T < T_U$ in-plane structure is ordered in the commensurate $p(\sqrt{7}\times\sqrt{7})R\,19.1°$ superlattice, where $T_U = 170$ K for $n = 2$, and decreases with increasing stage index. As the sample is heated above T_U, a reversible transition occurs to another ordered phase, which persists up to the transition temperature $T_m = 620$ K, above which a very complicated spot diffraction pattern is observed. At low temperatures ($T \sim T_U$), the bright-field real-space micrographs show a large number of small (~40-Å) regions that are highly absorbing to the electron beam, and are identified with clusters containing Rb. A dramatic and reversible change in the cluster size and shape occurs near the transition between the two ordered structures ($T \sim T_U$). An anomaly in the resistivity has also been reported for stage-2 graphite-Rb for $T_U = 172$ K.[26] It would be of particular interest to carry out further x-ray-diffraction studies on graphite-Rb and electron-diffraction studies on graphite-K to verify that the transition above T_U is to another ordered phase for the Rb compounds and to a disordered phase for the K compounds.

ACKNOWLEDGMENTS

We would like to thank Professor J. B. Vander Sande and Professor A. N. Berker for helpful discussions and Dr. A. Garrett-Reed for help with the experiments. We gratefully acknowledge support from NSF Grant No. NSF-78-10858 for this work.

*Center for Materials Science and Engineering and Department of Electrical Engineering and Computer Science.

†Francis Bitter National Magnet Laboratory, supported by NSF.

[1]M. S. Dresselhaus, G. Dresselhaus, P. C. Eklund, and D. D. L. Chung, Mater. Sci. Eng. 31, 141 (1977).

[2]R. G. Nemanich, S. A. Solin, and D. Guérard, Phys. Rev. B 16, 2965 (1977).

[3]T. Inoshita, K. Nakao, and H. Kamimura, J. Phys. Soc. Jpn. 43, 1237 (1977).

[4]N. A. W. Holzwarth and S. Rabii, Mater. Sci. Eng. 31, 195 (1977); N. A. W. Holzwarth, L. A. Girifalco, and S. Rabii, Phys. Rev. B 18, 5190 (1978).

[5]G. R. Hennig, *Progress in Inorganic Chemistry*, edited by F. A. Cotton (Interscience, New York, 1959), Vol. 1, p. 125.

[6]M. S. Dresselhaus and G. Dresselhaus, in *Physics and Chemistry of Materials with Layered Structures: Intercalated Layer Materials*, edited by F. Lévy (Reidel, Dordrecht, 1979), Vol. 6, p. 423.

[7]G. S. Parry, Mater. Sci. Eng. 31, 99 (1977).

[8]D. E. Nixon and G. S. Parry, Br. J. Appl. Phys. 1, 291 (1968).

[9]G. S. Parry and D. E. Nixon, Nature (London) 216, 909 (1967).

[10]G. S. Parry, D. E. Nixon, K. M. Lester, and B. C. Levene, J. Phys. C 2, 2156 (1969).

[11]W. T. Eeles and J. A. Turnbull, Proc. R. Soc. London, Ser. A 283, 179 (1965).

[12]J. A. Turnbull and W. T. Eeles, Proceedings of the 2nd Conference on Industrial Carbons and Graphite, Soc. Chem. Ind. London, 1966, p. 173.

[13]M. K. Halpin and G. M. Jenkins, Proceedings of the 3rd Conference on Industrial Carbons and Graphite, Soc. Chem. Ind. London, 1970, p. 53.

[14]E. L. Evans and J. M. Thomas, J. Solid State Chem. 14, 99 (1975).

[15]W. D. Ellenson, D. Semmingsen, and J. E. Fischer, Mater. Sci. Eng. 31, 137 (1977).

[16]W. Rüdorff and E. Schulze, Z. Anorg. Allg. Chem. 277, 156 (1954).

[17]D. Guérard and A. Hérold, Carbon 13, 337 (1975).

[18]N. Kambe, M. S. Dresselhaus, G. Dresselhaus, S. Basu, A. R. McGhie, and J. E. Fischer, Mater. Sci. Eng. 40, 1 (1979).

[19]A. W. Moore, *Chemistry and Physics of Carbon*, edited by P. L. Walker and P. A. Thrower (Dekker, New

York, 1973), Vol. 11, p. 69.
[20]B. Hirsch, A. Howie, R. B. Nicholson, D. W. Pashley, and M. J. Whelan, *Electron Microscopy of Thin Crystals* (Butterworths, London, 1965), Chap. 6.
[21]G. S. Parry, Proceedings of the 3rd Conference on Industrial Carbons and Graphite, Soc. Chem. Ind. London, 1970, p. 58.
[22]D. D. L. Chung, G. Dresselhaus, and M. S. Dresselhaus, Mater. Sci. Eng. 31, 107 (1977).
[23]D. D. L. Chung, Ph.D. thesis, MIT, 1977 (unpublished).
[24]R. Clarke, N. Caswell, S. A. Solin, and P. M. Horn, Phys. Rev. Lett. 43, 2018 (1979).
[25]J. B. Hastings, W. D. Ellenson, and J. E. Fischer, Phys. Rev. Lett. 42, 1552 (1979).
[26]D. G. Onn, G. M. T. Foley, and J. E. Fischer, Mater. Sci. Eng. 31, 271 (1977); Phys. Rev. B 19, 6474 (1979).
[27]In the schematic diagrams of this paper, the diffraction spots associated with the graphite structure are denoted by open circles.
[28]The symbol *o* refers to an oblique unit cell, with unit vectors for the $o(\sqrt{39}\times\sqrt{39})R(16.1°, 43.9°)$ structure given by:

$$\hat{a}_1^{(\sqrt{39})} = -5\hat{a}_1^{(1)} - 7\hat{a}_2^{(1)} = a_0(\sqrt{3}, -6, 0)$$

and

$$\hat{a}_2^{(\sqrt{39})} = 5\hat{a}_1^{(1)} - 2\hat{a}_2^{(1)} = a_0(7\sqrt{\tfrac{3}{2}}, \tfrac{3}{2}, 0).$$

[29]S. Y. Leung, C. Underhill, G. Dresselhaus, T. Krapchev, R. Ogilvie, and M. S. Dresselhaus, Solid State Commun. 32, 639 (1979).
[30]The coexistence of different ordered structures has been derived in a theory for commensurate adsorption to the basal graphite surface (S. Ostlund and A. N. Berker, Phys. Rev. B (to be published).
[31]Clusters have been previously reported in real-image studies of graphite intercalation compounds: refer to R. M. Fisher, D. J. Smith, L. A. Freeman, S. J. Pennycook, and A. Howie, 14th Biennial Conference on Carbon, Extended Abstracts, Pennsylvania State University, 1979, p. 318 (unpublished); for residue compounds, refer to Refs. 13, 14.
[32]P. Bak and E. Domany, Phys. Rev. B 20, 2818 (1979).
[33]R. Clarke, N. Caswell, and S. A. Solin, Phys. Rev. Lett. 42, 61 (1979).

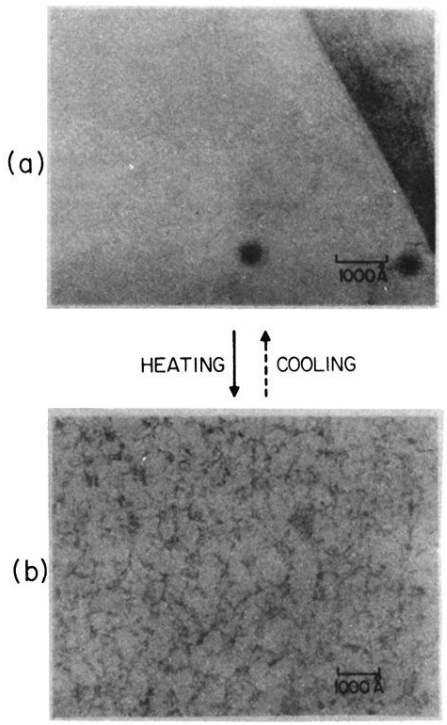

FIG. 10. (a) Bright-field image for a stage-2 graphite-Rb compound taken at 110 K. This micrograph is typical of low-temperature electron micrographs taken for $T < T_0 \simeq T_U$ ($T_0 = 160$ K and $T_U = 170$ K). We identify the dark areas with small clusters of ~40-Å diameter. (b) Bright-field image taken on the same spot of the sample as in (a), but at $T = 223$ K ($> T_U$). Larger clusters of ~180-Å diameter and channels are found for micrographs above T_U. A reversible variation in the cluster size between (a) and (b) is indicated by both straight and broken arrows, respectively, denoting heating and cooling processes.

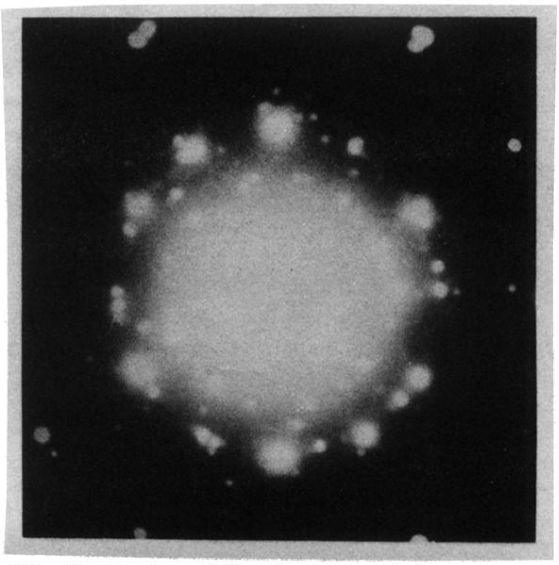

FIG. 12. Electron-diffraction pattern taken on a stage-2 Rb compound at 659 K, showing a very complicated intercalate arrangement. The multitude of diffraction spots and the bright halo are both associated with scattering by the intercalant. The graphite spots are undisturbed, but difficult to distinguish from the background.

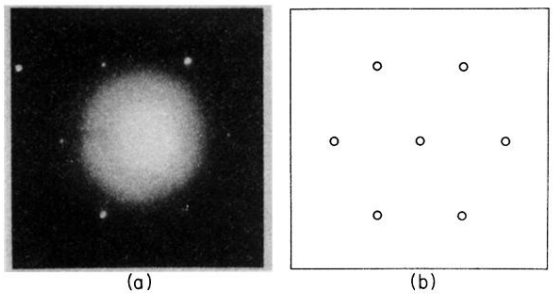

FIG. 3. (a) In-plane electron diffraction pattern for a well annealed stage-1 graphite-Rb (C_8Rb) sample for $T \lesssim 300$ K. (b) A schematic representation of the diffraction pattern in (a). The open circles denote the graphite pattern. The absence of a superlattice pattern indicates that the diffraction pattern for the intercalate is coincident with that for the graphite. This diffraction pattern is consistent with the sequential $\alpha, \beta, \gamma, \delta$ intercalate layer stacking of Fig. 1(a) and the sequential α, β, γ intercalate layer stacking of Fig. 1(b).

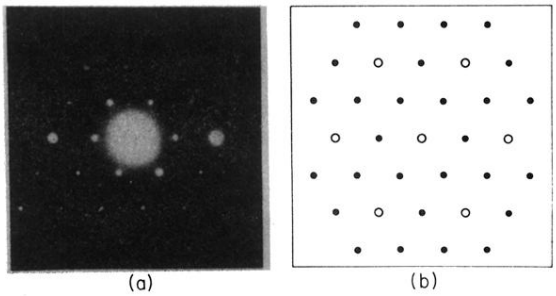

FIG. 4. (a) In-plane electron diffraction pattern for an as-grown stage-1 graphite-Rb (C_8Rb) sample and also for a well annealed stage-1 graphite-Rb (C_8Rb) sample for $T \gtrsim 300$ K. (b) A schematic representation of the diffraction pattern in (a). The superlattice structure indicated by the closed circles is consistent with a random arrangement of intercalate layers each having either α, β, γ, or δ site occupations.

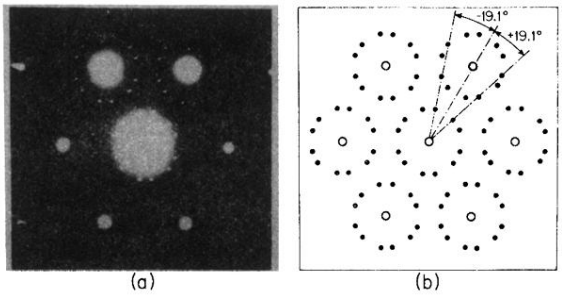

FIG. 5. (a) Low-temperature ($T < 170$ K) in-plane electron-diffraction pattern for graphite-Rb sample of stage $n = 2$. Similar patterns have been observed at low temperatures for samples with stages $n = 3, 4, 7$. (b) A schematic representation of the diffraction pattern in (a). This diffraction pattern shows two hexagonal superlattices rotated by $\pm 19.1°$ relative to the graphite lattice, and commensurate with the graphite lattice.

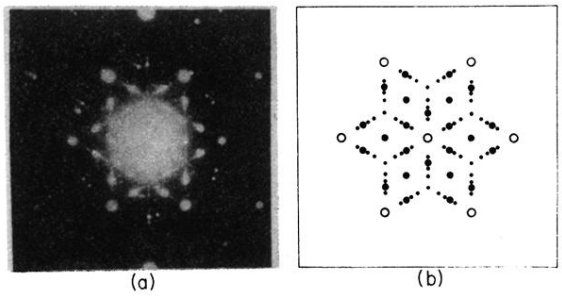

FIG. 7. (a) High-temperature ($170 < T < 620$ K) in-plane electron-diffraction pattern for stage-2 graphite-Rb samples (and referred to by $C_{\nabla}X$ in the text). Similar patterns are observed for samples with stages $n = 3, 4, 7$. (b) A schematic representation of the diffraction pattern in (a). The open circles refer to the graphite pattern, the large solid circles to intense superlattice spots, and the small circles to weak superlattice spots.